Journal of Structural Geology 168 (2023) 104827

Contents lists available at ScienceDirect

Journal of Structural Geology

journal homepage: www.elsevier.com/locate/jsg

The role of antithetic faults in transferring displacement across contractional relay zones on normal faults

Giovanni Camanni [a,b], Conrad Childs [b,c,*], Efstratios Delogkos [b], Vincent Roche [b,c], Tom Manzocchi [b,c], John Walsh [b,c]

[a] DiSTAR, Università degli Studi di Napoli "Federico II", Naples, Italy
[b] Fault Analysis Group, UCD School of Earth Sciences, University College Dublin, Belfield, Dublin 4, Ireland
[c] Irish Centre for Research in Applied Geosciences (iCRAG), UCD School of Earth Sciences, University College Dublin, Belfield, Dublin 4, Ireland

A B S T R A C T

Contractional relay zones between pairs of normal faults are sometimes associated with multiple antithetic faults in a geometry similar to that found in Riedel shear zones. Detailed fault displacement profiles of outcrop examples of this geometry demonstrate that the antithetic faults accommodate the transfer of displacement between the synthetic faults that bound the relay zones. The throw on individual antithetic faults, or R′ shears, is typically constant across relay zones while the throw profile on the synthetic faults, or R shears, is stepped; the steps occurring across branchpoints with abutting R' shears. Transfer of fault displacement occurs by a combination of block rotation and irrotational block translation within the relay zone. As fault throw increases, contractional relay zones are by-passed by the linkage of the synthetic faults, in a manner analogous to the formation of P-shears by the linkage of R shears in classic Riedel shear experiments, but with the original relay zone structure still preserved within the fault zone. With yet further strain bedding may rotate into near-parallelism with the fault surface, with the original geometrical configuration of the relay zone difficult to unravel.

1. Introduction

Brittle shear zones and incipient fault zones commonly comprise two sets of minor faults (e.g., Tchalenko, 1970; Naylor et al., 1986; Richard et al., 1995; Ahlgren, 2001; Pennacchioni and Mancktelow, 2013; Nabavi et al., 2020; Camanni et al., 2021). The first is a set of 'synthetic' faults with the same sense of offset as the overall structure

These are frequently a series of en-echelon segments at a low angle to the overall structure (Fig. 1A). The second set are 'antithetic' faults that have the opposite sense of shear and are at a high angle to the overall structure (Fig. 1A). This arrangement of syn- and antithetic faults has been described in a wide range of settings and scales and, most frequently, for map views of strike-slip faults (Fig. 2A, B, C) both at regional (Nicholson et al., 1986; Pucci et al., 2007; Faulkner et al., 2003, 2008; Cembrano et al., 2005; Carpentier et al., 2012; Stanton-Yonge et al., 2020) and at outcrop (Kim et al., 2003; Pennacchioni and Mancktelow, 2013) scales and is common in surface ruptures of strike-slip earthquakes (e.g., Tchalenko and Ambraseys, 1970; Terres and Sylvester, 1981; Quigley et al., 2010, 2012; Ren et al., 2021, Fig. 2A and B). The same patterns of faults can be recognised in cross-sections of dip-slip fault systems in both contractional (Fig. 2D, Arboleya and Engelder, 1995), and extensional (Fig. 2E, F, G, H; Mandl, 1987; Ferrill and Morris, 2008; Ferrill et al., 2009, 2011; Childs et al., 2009; Zaky, 2017; Nixon et al., 2018; Nabavi et al., 2020; Camanni et al., 2021) settings. A similar pattern has been widely recognised in deformation bands developed in porous sandstone irrespective of the mode of faulting (Fig. 2E and F): pairs of synthetic deformation bands, commonly bound a series of antithetic deformation bands, referred to as "linking bands" by Schultz and Balasko (2003), both combining to define an array referred to as a "ladder" geometry (e.g., Antonellini and Aydin, 1995; Davis, 1999; Davis et al., 2000; Ahlgren, 2001; Schultz and Balasko, 2003; Katz et al., 2004; Okubo and Schultz, 2005; Tondi et al., 2006).

In the typical arrangement shown in Fig. 1A, adjacent synthetic faults are arranged in an en-echelon geometry. The zones of overlap between the faults have a contractional strain, and in the literature have been variously termed transfer zones, overlap zones, overstep zones, stepover zones or relay zones. In this paper they are referred to as contractional relay zones (e.g., Camanni et al., 2019; Delogkos et al., 2020; Roche et al., 2020, 2021; Diamanti et al., 2022). The locations of the antithetic faults are often confined to the contractional relay zones (Figs. 1B and 2), and contractional relay zones containing antithetic faults have been described in many different fault systems (e.g., Arboleya and Engelder, 1995; Schultz and Balasko, 2003; Childs et al., 2009; Pennacchioni and Mancktelow, 2013; Nabavi et al., 2020, Fig. 2). The

* Corresponding author. Fault Analysis Group, UCD School of Earth Sciences, University College Dublin, Belfield, Dublin 4, Ireland.
E-mail address: conrad.childs@ucd.ie (C. Childs).

https://doi.org/10.1016/j.jsg.2023.104827
Received 4 May 2022; Received in revised form 25 December 2022; Accepted 15 February 2023
Available online 17 February 2023

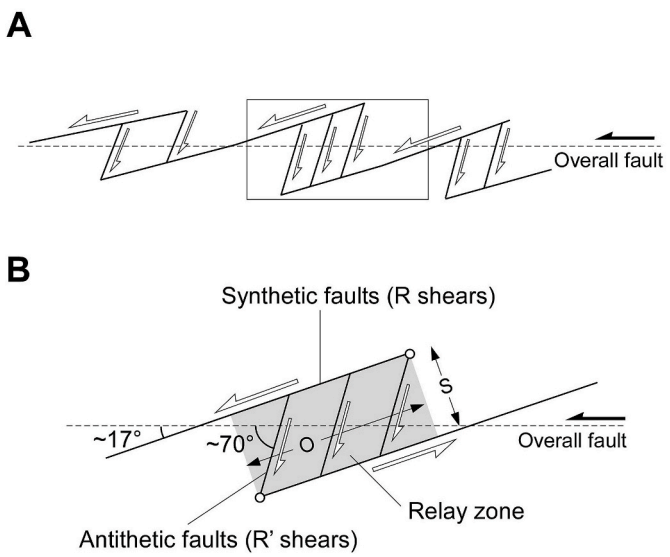

Fig. 1. A: Typical map pattern of brittle shear zones and incipient fault zones (redrawn after an early analogue model of strike-slip faults from Wilcox et al., 1973), showing two sets of minor faults, synthetic and antithetic to the overall fault. **B**: Contractional relay zone highlighting the minor faults (R and R' shears) and their angular relationships with the strike of the overall fault (redrawn after Naylor et al., 1986). O: relay zone overlap; S: relay zone separation.

antithetic faults have been suggested to play a role in transferring fault displacement between synthetic faults (Childs et al., 2009; Nixon et al., 2018; Zaky, 2017; Nabavi et al., 2020; Camanni et al., 2021). However, detailed accounts of the displacement distribution within these zones of syn- and antithetic faulting that either quantitatively demonstrate this or shed light on the mechanism of displacement transfer are rare (but see Pennacchioni and Mancktelow, 2013). This article presents detailed descriptions of the displacement distribution on synthetic and antithetic faults at contractional relay zones between pairs of overlapping normal faults. The analysed normal fault zones have centimeter to 100 m fault displacements and offset many sedimentary layers so that detailed displacement profiles can be constructed to constrain the mode of displacement transfer across the relay zones.

Bed rotations in sympathy with the sense of shear on the synthetic fault segments is characteristic of contractional relay zones between normal faults (Mandl, 1987; Ferrill and Morris, 2008; Ferrill et al., 2009; 2011; Childs et al., 2009; Zaky, 2017; Nixon et al., 2018; Nabavi et al., 2020; Camanni et al., 2021). Bed rotation is a feature of most of the examples considered here and is incorporated into a model for the evolution of these characteristic fault patterns to high strain. While all of the examples considered are for normal faults, we consider that the geometric analysis enabled by these normal faults is relevant to similar fault patterns in other modes of faulting.

2. Terminology, data and methods

2.1. Terminology

This paper is concerned with pairs of synthetic faults with overlapping Mode II tips in a contractional arrangement and associated, high angle, antithetic faults (Fig. 1). This arrangement of faults is the same as that observed in the classic Riedel shear geometry, originally generated in analogue models of faulting above a basement strike-slip fault (Cloos, 1928; Riedel, 1929; Tchalenko, 1970; Wilcox et al., 1973; Naylor et al., 1986; Richard et al., 1995; see Dooley and Schreurs, 2012, for a comprehensive review). The Riedel shear terminology, in which synthetic faults are referred to as R shears and antithetic faults as R′ shears has been widely used to describe natural examples of faults of the types described in this work regardless the mode of faulting (e.g., among others, Arboleya and Engelder, 1995; Katz et al., 2004; Quigley et al., 2010, 2012; Camanni et al., 2019; Ren et al., 2021). We follow these papers in using the terminology to describe an arrangement of R and R' shears within a Riedel geometry (Fig. 1B) but acknowledge that the boundary conditions and mechanics of these faults may be very different to those of the classic Riedel experiments. The relay zone dimensions are defined by separation (S), which is the distance between overlapping R shears measured perpendicular to the fault, and length (O), which is the length of overlap between R shears (Fig. 1B).

2.2. Data

This paper is based on analysis of structures from normal faults in three areas: the Ptolemais area of NW Greece, the Moab area in SE Utah (USA), and the Buzi Range area in Southern Pakistan. Examples of structures from each area are presented to provide a range of fault styles and scales of observation. Detailed mapping of two particularly well-exposed examples is presented to illustrate the systematics of fault displacement distribution in contractional relay zones with a Riedel geometry.

Ptolemais area: Lignite mining in the Ptolemais Basin, NW Greece, provides extensive outcrop of a system of Quaternary normal faults offsetting the early Pliocene Ptolemais Formation, a lacustrine sequence of alternating lignites and marls with occasional clay and sand intervals (Pavlides and Mountrakis, 1987, 1987a, 1987b; Pavlides and Mountrakis, 1987;b, 2018). The combination of 20 m high mine faces and alternating black lignite and white marl provides many highly photogenic examples of contractional relay zones. Whilst partial exposures of large scale examples of Riedel fault geometries occur (e.g. Delogkos et al., 2020), the examples presented here are small and entirely contained within a single mine face (Fig. 3A to **C, 4)**. The particular examples presented here no longer crop out, as mining has advanced and the mine faces have been excavated but similar structures are regularly exposed.

Moab area: Riedel shear geometries at contractional relay zones are very commonly observed in the Moab area of SE Utah (Fig. 3D–H). High vertical cliff sections (100's m) expose normal faults that cut massive sandstone units of Jurassic age (Foxford et al., 1996, 1998; Gent and Urai, 2019). Riedel geometries have previously been described for deformation bands in these rocks (e.g., Davis et al., 2000; Ahlgren, 2001) but similar geometries between discrete faults are also very common on a wide range of scales (Fig. 3D–H).

Buzi Range area: Extensional faulting within the Buzi Range area, S Pakistan, initiated during deposition of the Late Miocene to Pliocene Talar Formation, made up of medium-to coarse-grained sandstones, interbedded with shales and mudstones deposited in a deltaic environment (Ellouz-Zimmermann et al., 2007; Back and Morley, 2016). The normal fault offsets measured here are within the pre-faulting rather than the syn-faulting sequence. Following deposition, development of the Makran fold and thrust belt (e.g., Platt et al., 1988; Back and Morley, 2016) resulted in folding of the Talar Formation. The area studied here lies on the northern limb of the Hinglay Syncline with bed dips of ~30° and sediments younging towards the south (Back and Morley, 2016). Hence, the Talar Formation is now exposed as a section oblique to both bedding and the extension direction, and the normal faults have apparent strike-slip offsets (Fig. 5; Back and Morley, 2016). Despite the significant post-faulting deformation, normal faults in this area are thought to preserve their original geometries and normal fault displacements (Back and Morley, 2016). The relay zone from this area (Fig. 5) is the largest presented in this paper and has a separation of ca. 400 m, an overlap length of ca. 1 km, and a total throw of 90 m.

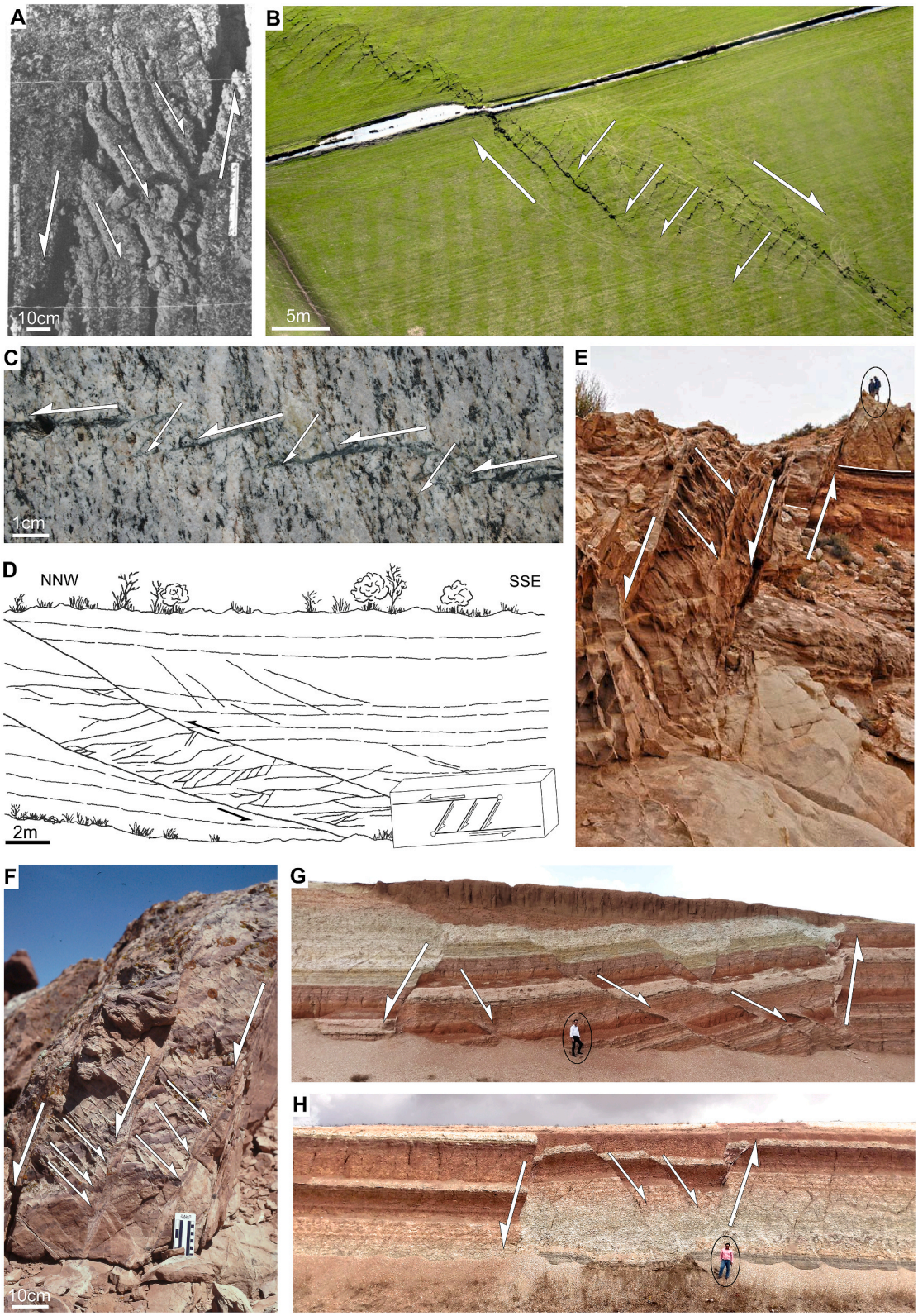

Fig. 2. Examples of Riedel-like geometries (*sensu* Tchalenko, 1970) in nature developed in strike-slip (**A**: A portion of the surface rupture of the 1979 Imperial Valley earthquake in USA, modifed after Terres and Sylvester, 1981; **B**: Part of the surface trace of the 2010 Darfield earthquake in New Zealand, modifed after Quigley et al., 2010, 2012; **C**: modifed after Pennacchioni and Mancktelow, 2013), reverse (**D**: modifed after Arboleya and Engelder, 1995), and extensional faults (**E**: Goblin Valley, Utah, USA - courtesy of Haakon Fossen; **F**: modifed after Antonellini and Aydin, 1995; **G, H**: modifed after Nabavi et al., 2020). **E** and **F** are examples of deformation bands developed along normal faults in porous sandstone. See main body of the text for further descriptions. Note that the sense of slip of faults shown by the annotations (arrows) in these figures is not always expicitily described in the original publications.

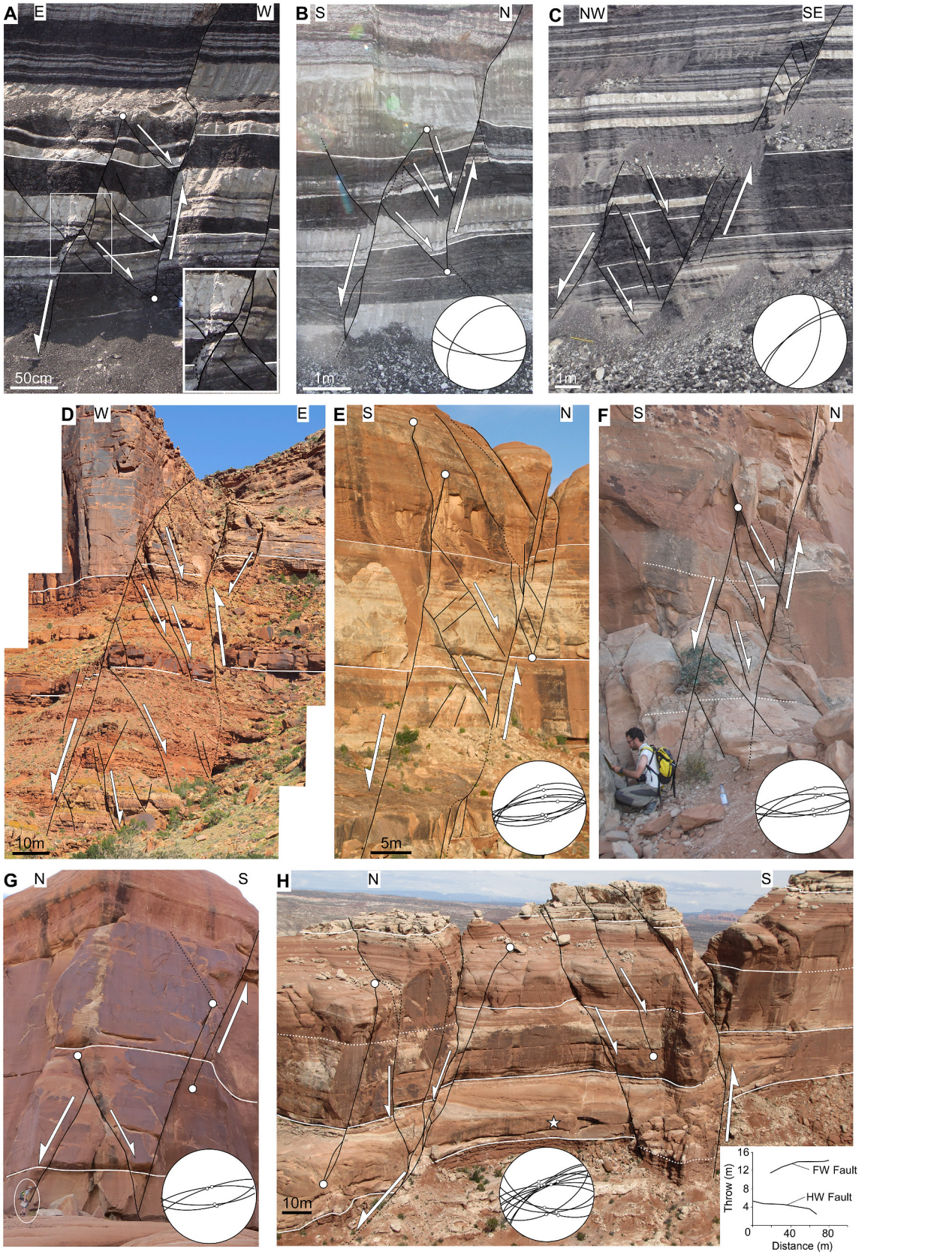

(caption on next page)

Fig. 3. Contractional relay zones developed in normal faults observed on cross-section showing a structure equivalent to that of Riedel shear zones and displaying an internal structure defined by antithetic faults and variably accentuated synthetic bed rotation. **A, B, C**: Ptolemais Basin, Greece; **D, E, F, G, H**: Moab area, Utah. Bedding in **E, F, G, H** is gently dipping at ca. 5–6° towards the N-NW. Where available, fault plane orientation data and their slip vectors recorded as slickenlines on the fault surfaces are shown (dot on the faults in the plots indicate the trend and the plunge of the direction of movement of the downthrowning hangingwall fault block). In these examples, throw transfer between fault segments bounding the relays can be inferred by the downward decrease in throw on the footwall fault segments accompanied by the reciprocal downward increase in throw on the hangingwall ones. For the example in **H**, a throw profile is used to show this (starting point for measuring "distance" in this profile is located at the bottom of the outcrop near the location of the white star, and "distance" is measured upward from this point). **G** is an exception to this, as the throw is nearly null across the fault zone at outcrop. Location data in latitude-longitude of the examples from the Moab area: **D**, 38°38′57.82″N-109°30′35.40″W; **E**, 38°42′32.83″N-109°43′44.55″W; **F**, 38°42′33.79″N-109°43′44.53″W; **G**, 38°42′33.72″N-109°43′46.95″W; **H**, 38°42′26.15″N-109°43′45.70″W.

2.3. Throw profile construction

Two exceptionally well-exposed examples of fault zones displaying Riedel geometries have been selected for detailed fault displacement analysis, one from the Ptolemais area (Fig. 4) and one from the Buzi Range area (Fig. 5). Both examples offset sedimentary layers that are thin compared to the relay zone overlap and that can be correlated across and within the relay zone so that significant numbers of markers allow construction of detailed throw (i.e., vertical displacement) profiles. The interpretations of the relay zones in Figs. 4 and 5 show only a subset of the horizons used; the analysis and the full interpretations are provided in the supplementary material (Figs. S1 and S2).

This study is based on throw (or apparent throw) rather than displacement measurements because throw is largely unaffected by either minor irregularities in fault trace geometry due to the irregularity of the exposure or small differences in the orientation of fault surfaces relative to the plane of inspection. Throw values are calculated for each horizon as the vertical distance between the footwall and the hangingwall cut-off points across the same fault so that measures are independent of differences in bed dip between the footwall and the hangingwall layers. Calculated throw values were measured on a scaled photo taken in the field for the Ptolemais area (Fig. 4 A) and on a scaled

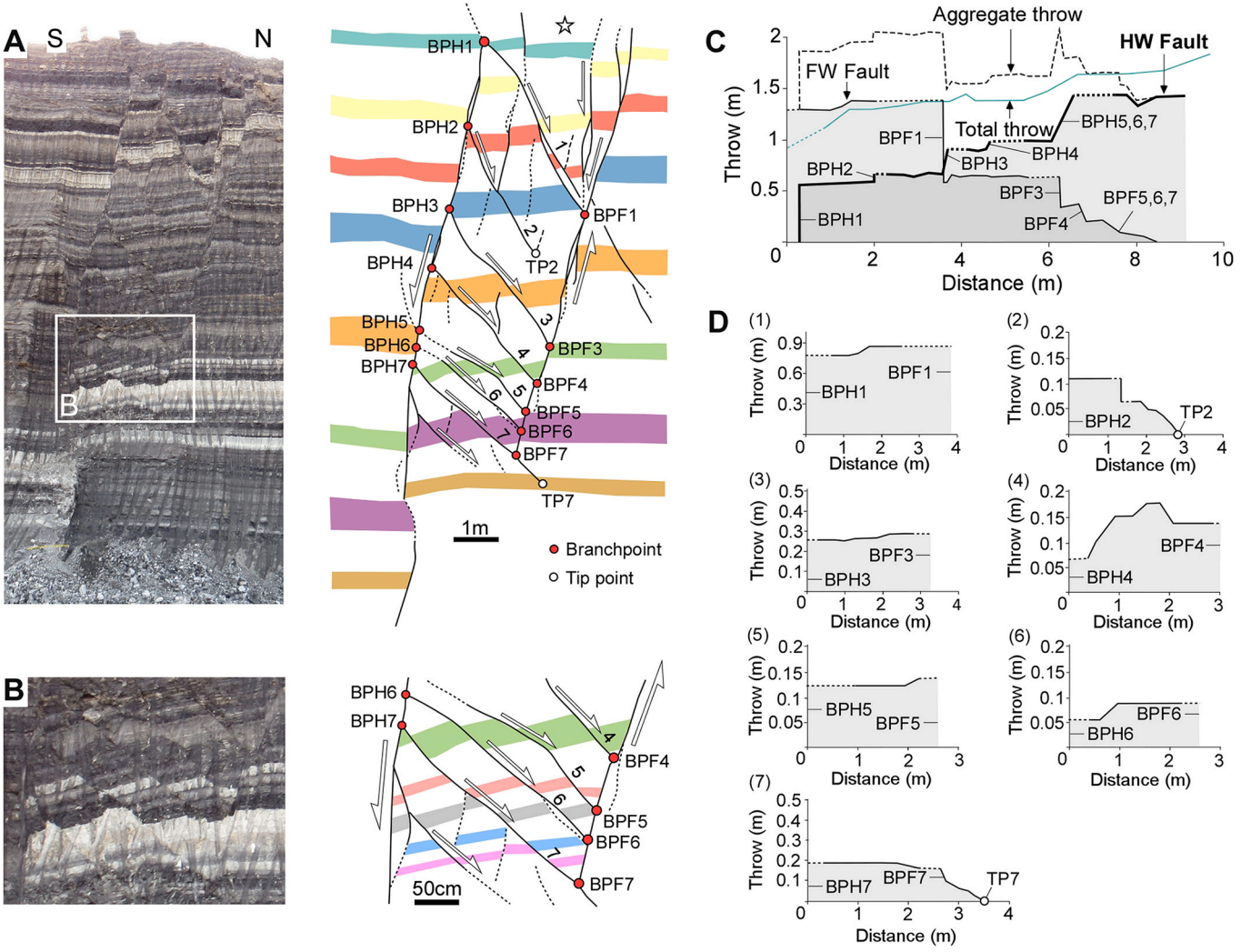

Fig. 4. Relay zone from the Ptolemais Basin area (Greece), with the relay area defined by antithetic faulting and synthetic bed rotation. **A**: uninterpreted photo (and interpretation on the side) of the whole relay zone; **B**: uninterpreted detail photo (and interpretation on the side) of the lower portion of the relay zone (see **A** for location); **C**: throw profiles of the faults bounding the relay zone (i.e., R shears); **D**: throw profiles of the antithetic faults within the relay zone (i.e., R′ shears). For the construction of the detailed throw profiles shown in **C** and **D**, many more layers than those shown in **A** and **B** have been used: throws of 38 layers have been measured and used for constructing the throw profiles (see Supplementary Fig. S1).

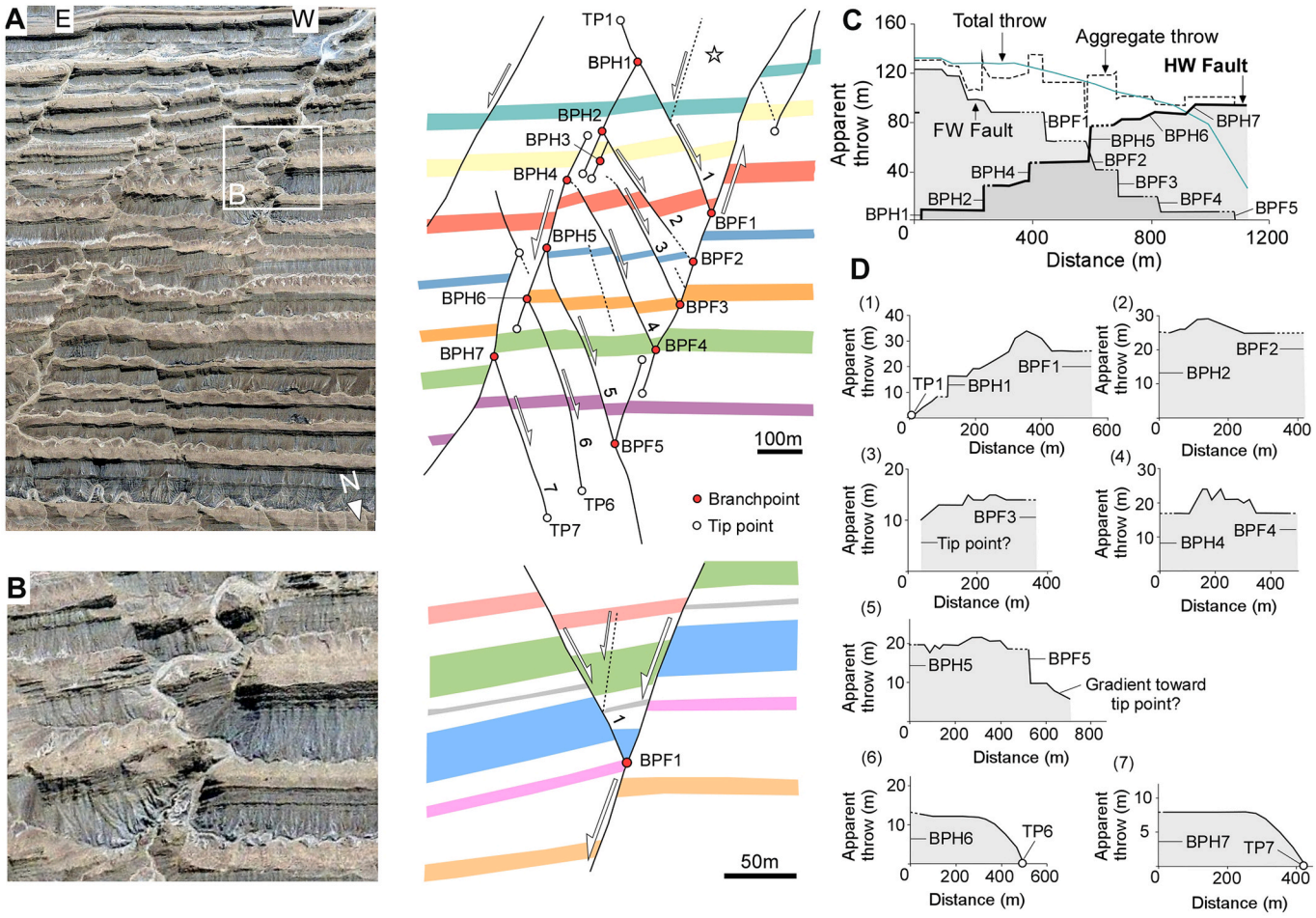

Fig. 5. Relay zone from the Buzi Range area (Pakistan), as imaged from satellite imagery data (ESRI 1 m resolution World Imagery data; the original image was rotated for consistency with the other figures of the article). Note how the relay area is defined by antithetic faulting and synthetic bed rotation. **A**: uninterpreted satellite image (and interpretation on the side) of the whole relay zone; **B**: uninterpreted detail image (and interpretation on the side) of a branchpoint area between the footwall fault bounding the relay zone and an antithetic fault within it (see **A** for location); **C**: throw profiles of the faults bounding the relay zone (i.e., R shears); **D**: throw profiles of the antithetic faults within the relay zone (i.e., R′ shears). For the construction of the detailed throw profiles shown in **C** and **D**, many more layers than those shown in **A** and **B** have been used: throws of 45 layers have been measured and used for constructing the throw profiles (see Supplementary Fig. S2). Location data in latitude-longitude: 25°28′2.62″N-65°11′11.43″E.

image extracted from satellite data for the Buzi Range area (Fig. 5 A). For the Ptolemais example, where the mine faces are approximately vertical and bedding is flat-lying (i.e., normal to the plane of inspection), throw values are real. For the Buzi Range area the bed dip is ~30° (Back and Morley, 2016) towards the south (i.e., at an angle with the plane of inspection) so that the measured throws are apparent and are systematically higher than the actual throw (Fig. 5). However, as there is no significant change in bed dip magnitude over the detailed study area, the proportions of offset accommodated by different faults are unaffected.

Throw profiles are plotted as a function of distance parallel to the individual fault traces for both the R and R′ shears. Measured throw values can be located at the footwall or hangingwall cut-off points, or at the mid-point between them. In this article, we locate readings at the mid-point but the other methods are occasionally used so that readings can be placed nearer to a branch point. The origin for the profiles of the relay-bounding R shears (Figs. 4C and 5C) is placed at the top of the relay zone (the stars in Figs. 4A and 5A, and Figs. S1 and S2). The origin for each R' shear (Figs. 4D and 5D) is its upper branch or tip point. Aggregate throw profiles were generated by summing up the two profiles of the relay-bounding R shears. Total throw is calculated for each horizon as the difference in elevation of horizon cut-offs outside the relay zone, i.e. between the footwall cut-off on the footwall fault and the hangingwall cut-off of the hangingwall fault. In all cases throws derive from all layers examined (see Figs. S1 and S2) and not just those shown in Figs. 4 and 5.

The following section examines the geometry, kinematics and structural relationships between R and R' shears with reference to the examples presented in Figs. 3, 4 and 5. The detailed fault displacement analyses of the two examples introduced above (Figs. 4 and 5), are described in Section 4.

3. Geometry and kinematics

Examples of vertical exposures of contractional relay zones from the Ptolemais and Moab areas are shown in Fig. 3. These all show Riedel shear zone geometries consisting of two synthetic faults (R shears) stepping in a contractional sense and bounding a rock volume that is offset by one or more antithetic faults (R' shears). In each case the displacement variations along the R shears are complementary, with displacement decreasing upwards on the hangingwall fault and increasing upwards on the footwall fault. This transfer of displacement is apparent from inspection of the photographs Fig. 3 A to F. Fig. 3H shows a 140 m wide fault zone, dipping to the north, that is interpreted to represent a portion of a larger contractional relay zone. Throw profiles constructed from the 100 m high cliff exposure (Fig. 3H inset) demonstrate the transfer of throw between the faults that bound the zone, and

extrapolation of these profiles suggests that the relay zone has a vertical extent of ca. 300 m.

R shears bounding the relay zones are always broadly parallel to one another (Fig. 3). Slickenlines of quartz fibres on fault surfaces in the Moab area show the direction of slip (Fig. 3E to H). Usually, these slip vectors show dominantly dip-slip movement on both R and R′ shears which have similar strikes to each other and therefore sub-horizontal lines of intersection (e.g. Fig. 3E and G). In cases where the slip vectors are inclined on both sets of shears (e.g., Fig. 3F) there is a systematic misalignment of fault strike, resulting in lines of intersection between the R and R' shears that are perpendicular to the slip vectors (i.e., slightly inclined). It is worth noting that in the area of Fig. 3F the bedding is locally gently dipping towards the N-NW (5–6°), a bed rotation that would not provide the observed westward tilt (as seen in Fig. 3F) of an originally sub-horizontal line of intersection. It is more likely, therefore, that the faults in the Moab area were not pure dip-slip from the inception, and that the slip vector within the contractional relay zones was always perpendicular to the slightly inclined line of intersection between the conjugate shears (see also Gent and Urai, 2019 for additional slip vector measurements in this area).

In the Ptolemais area the relative orientations of the R and R' shears are more variable and, although the regional bedding is everywhere sub-horizontal, the lines of intersection between the conjugate shears may plunge by up to 40° (Fig. 3B and C). Kinematic indicators in the form of fault surface striations are rare in the Ptolemais mines. Where present they indicate dip-slip movement but good examples of contractional relay zones with striated fault surfaces were not found. By analogy with the structures in the Moab area we would, however, expect that fault slip vectors are normal to the lines of intersection between the conjugate shears.

Synthetic rotation of bedding between adjacent R′ shears is common (e.g., Figs. 2G, 3B and 4A, 5A) and the largest bed rotations within a zone are associated with the lowest R′ shear dips. Examples of this relationship are the two antithetic faults on the right-hand side of the fault zone in Fig. 2G, the lowermost antithetic fault in Fig. 3B, antithetic faults 5, 6, 7 in Fig. 4A, and antithetic fault 2 in Fig. 5A. This geometric relationship is reminiscent of a bookshelf style of faulting and suggests that throw on an individual R′ shear can be achieved through a synchronous synthetic rotation of both the fault itself and bedding (e.g., Mandl, 1987; Tapponnier et al., 1990). Bed rotation is not ubiquitous and the absence of significant synthetic bed rotation in other relay examples such as those developed in Moab (Fig. 3 D to H), as well as some of those developed in Ptolemais (e.g., Fig. 3A and C), suggests that bed rotation between and adjacent to R' shears is not a geometric requirement and throw transfer can take place in its absence (see section 5.2). However, we anticipate that bed rotation is a ubiquitous component of fault structure at high strains (see discussion section).

There is a broadly constant ratio between the spacing of R′ shears and the relay zone separation. The two faults shown in Fig. 3C and E, for example, each contain two different sized relay zones with the smaller separation zones containing more closely spaced R′ shears. For the faults inspected here the spacing between R' shears is typically about one half to one quarter (i.e., 0.5–0.25) of the relay zone separation (Figs. 3–5), however this ratio is also likely to be a function of the rock properties of the faulted sequence. For example, when similar geometries develop in deformation bands within porous sandstones, spacings between the antithetic structures can be much smaller than the separation between the bounding deformation bands (i.e., 0.25 to < 0.1; Fig. 2E and F).

Several different geometrical relationships between individual R and R′ shears are observed (Fig. 6). The most common relationship is one in which an R′ shear abuts against an R shear (Figs. 3–5) and most R′ shears abut R shears at both ends so that they are confined within the relay zone (Fig. 6(1)). This relationship is strongly suggestive of a model in which R′ shears and the bounding R shears act together during displacement accumulation rather than through successive episodes of synthetic and antithetic fault activity. Examples of R′ shears that extend outside the relay zone and terminate at a tip point also exist (Fig. 6(2), (3)), indicating that relay-related deformation is not confined within the relay zone but can also extend outside of it; this observation has been made by previous authors (e.g., Nixon et al., 2018). R′ shears that extend outside the relay zone tend to occur at the top and bottom of the relay zone (see R′ shears 1 and 7 in Fig. 4A and B, and 1, 5, 6, 7 in Fig. 5A). In these cases the R shear may abut the R′ shear (e.g. Figs. 3G and 4A branchpoints BPH1 and BPF7, and Fig. 5A branchpoints BPH1 and BPF5; Fig. 6(2)). In the Ptolemais area, there are instances where both the R and R′ shears terminate at the same point to define a V-shape at a branchpoint (Fig. 3A–C). Generally, where they cross-cut one another, R shears offset R′ shears (e.g. Fig. 3B), but in a couple of examples R and R′- shears have mutually off-setting relationships. For example, in Fig. 3A the hangingwall R shear offsets an R′ shear but closer inspection (Fig. 3A inset) shows that the R shear splays towards the intersection and these splays are offset by the R′ shear in a geometry characteristic of conjugate faults (Nicol et al., 2013).

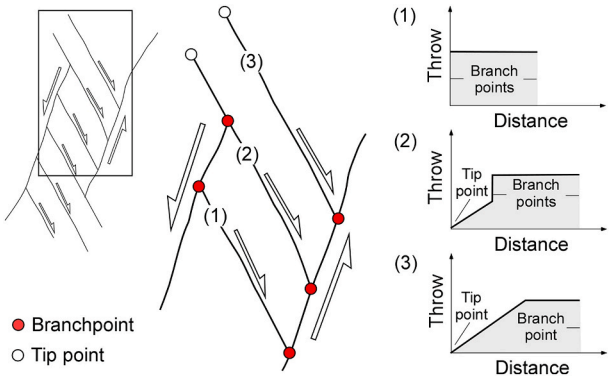

Fig. 6. Various types of R′ shears that can be recognised in the relay zones studied in this article. (**1**) R′ shears fully confined within the relay zone and linked to the R shear bounding the relay zone at two branchpoints; (**2**) R′ shears that extend and tip out outside the relay zone and are linked to the R shears bounding the relay zone at two branchpoints (one of the two branchpoints coinciding with the tip point of one of R shears bounding the relay zone); (**3**) R′ shears that extend and tip out outside the relay zone and are linked to the R shears bounding the relay zone at only one branchpoint.

The above geometrical observations all provide constraints on the development of contractional relay zones and the relative timings of the component faults and bed rotations. These observations will be synthesised with the following account of the throw distributions within selected relay zones as a prelude to defining a model for their geometrical evolution.

4. Fault displacement distribution

The distribution of throw along R and R′ shears and their interrelationships are described in this section. The focus is on detailed throw profiles constructed for the R and R' shears on two of the best examples of contractional relay zones, from the Ptolemais (Fig. 4) and the Buzi Range (Fig. 5) areas, although many of the features described can also be identified from close inspection of examples from the Moab area (Fig. 3).

4.1. Throw on R shears

The typical throw distribution associated with contractional relay zones is apparent from the throw profiles of the relay-bounding R shears in Figs. 4C and 5C, with a downward decrease in throw on the footwall fault broadly mirrored by a downward increase in throw on the hangingwall fault. Rather than the smooth throw profiles that are typically seen at neutral relay zones (e.g. Peacock and Sanderson, 1994), the hangingwall and footwall R shears bounding the relay zones (labelled

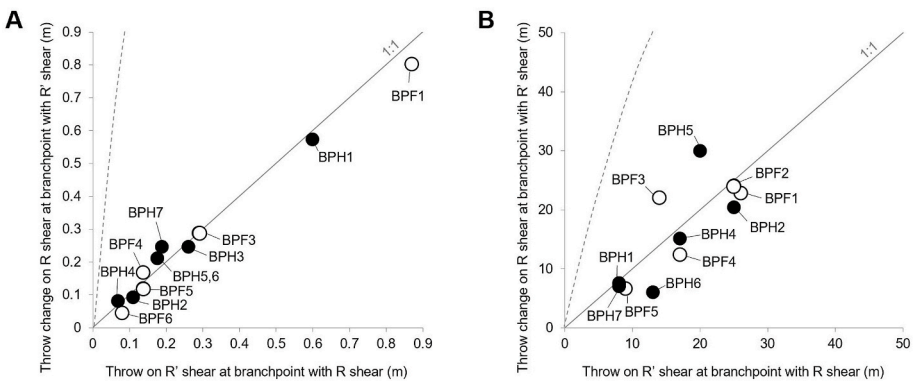

Fig. 7. Plots showing the relationships between the throw on R′ shears and the change in throw along the R shears at their branchpoint with the same R′ shear for the Ptolemais (**A**) and the Buzi Range (**B**) relay zones examined in Figs. 4 and 5, respectively. BPF (open circles) and BPH (filled circles) represent branchpoints on the footwall and hangingwall R shears, respectively. The dashed grey curves show ratios between these two parameters predicted by the construction illustrated in Supplementary Fig. S3 for block widths and initial fault dips of (**A**) 1.5 m and 75° and (**B**) 100 m and 66°

HW Fault and FW Fault in Figs. 4C and 5C) have stepped throw profiles where portions with near-constant throw alternate with steps in throw across branchpoints with R' shears (BPF and BPH in Figs. 4 and 5 indicate branchpoints on the footwall and hangingwall R shears). Hence, throw gradients on the relay-bounding R shears at the branchpoints are infinite, at least at the resolution provided by the data.

The aggregate throw profile of the R and R' shears is broadly constant but is irregular at scales that reflect the abrupt steps on the bounding faults. The profile of total throw, measured between horizon cut-offs on the relay-bounding R shears, describes a smooth variation in throw (Figs. 4C and 5C). The significance of the difference between the aggregate and total throw profiles is discussed below.

4.2. Throw on R' shears

As discussed in the previous Section 3 (e.g., Fig. 6), R′ shears may be confined within a relay zone or extend outside it. Most R′ shears that are confined within a relay zone (Fig. 6 (1)) have a near-constant throw along their length between their branchpoints with the footwall and hangingwall R shears (e.g., R′ shears 1, 3, 5, 6 in Figs. 4D, 2 and 3, 4 in Fig. 5D). However, some R′ shears display a slight variation in throw along their length with maximum values in their central portions (e.g., R′ shears 2, 4 in Fig. 5D). R′ shears that extend outside the relay zone (Fig. 6 (2 and 3)) again have near-constant throws within the relay zone but outside the relay zone the throw decreases progressively towards the tip with gradients much larger than those within the relay zone. If there is no intersection with the bounding R shear, then there is a simple increase in the throw gradient on the R′ shear at the margin of the relay zone (Fig. 6(3), R′ shears 6 and 7 in Fig. 5D), but if the R shear abuts the continuous R′ shear then there is a step decrease in the throw of the R′ shear at the branchpoint (Fig. 6(2), R′ shears 7 in Figs. 4D, 1 and 5 in Fig. 5D). Sharp throw changes can also occur along the lengths of the R′ shears across branchpoints with occasional subsidiary synthetic shears located within the relay zone (in a similar way to the sharp throw changes along the relay-bounding R shears; see, for example, R' shear 1, 2 and 4 in Fig. 4D).

4.3. Relationships between the magnitude of throw on R and R' shears

Of key significance in this study is the observation that the constant throws on individual R′ shears within a relay zone are similar in magnitude to the steps in throw on the bounding R shear(s) at the branchpoint with that same R′ shear. Fig. 7 plots R′ shear throw versus the magnitude of the change in R shear throw for branchpoints where R′ shears abut against R shears for the Ptolemais and Buzi Range examples. The individual branchpoints between R and R' shears are labelled in Fig. 7. The data show a general 1:1 correlation but with some outliers in the Buzi Range example (Fig. 7B). The outliers are largely attributable to data resolution in the Buzi Range area and also potentially to bed rotations out of the plane of observation. Overall, Fig. 7 is taken to indicate that, in general there is a 1:1 correspondence and this will be taken as a key constraint on the mechanism of fault displacement transfer across the relay zone in the next section.

5. Relay zone evolution

There are several published accounts of the stages of evolution of relay zones between normal faults as seen in map view (Peacock and Sanderson, 1994; Childs et al., 1995; Soliva and Benedicto, 2004). Three stages are usually identified: the initiation of the relay zone geometry, the transfer of fault displacement across the relay zone, and finally the breaching of the relay zone to form a throughgoing fault surface. This section describes these stages in the development of contractional relay zones with a Riedel geometry (Fig. 8) as constrained by the observations presented above. The description below is an idealisation based on the examples observed in the Ptolemais, Moab, and Buzi Range areas but is not intended to be a specific representation of the relay zones in any of these field areas which vary in detail.

5.1. Relay zone initiation

Abutting and cross-cutting relationships between R and R′ shears in the various examples presented provide clear constraints on the early evolution of these zones. A generalised initial geometry of these structures is illustrated in Fig. 8A with two R shears, with or without R'shears (dashed lines in Fig. 8A). It is possible that an R′ shear may extend outside the relay zone at one or both ends, as may have been the case in the example shown in Fig. 3B. The R shears may propagate to intersect with (e.g., Figs. 3G and 4 BPH1 and BPF7, Fig. 5 BPH1 and BPH5, footwall R shear in Fig. 8A), or cross-cut (e.g., Fig. 3A and B) earlier formed R′ shears. The conjugate fault geometry developed between the hangingwall R shear and the R′ shear in Fig. 3A demonstrates that both were active but that the R shear was the more recently active as shown by the continuity of the R shear through the conjugate structure.

It is worth noting that Segall and Pollard (1980) calculated stress distributions in the region between en-echelon fault segments in a contractional arrangement will promote the formation of antithetic shear fractures both within and outside of the zone of overlap (their Fig. 8A). While early initiation of R′ shears is therefore mechanically plausible, the outcrop evidence, in terms of the intersections between the R and R′ shears demonstrates that the R' shears formed within an already established zone of overlap. Using similar field relations to those observed here, Martel et al. (1988) concluded that 'the internal fractures of a fault zone are younger than its boundaries' including anthithetic shears.

5.2. Fault displacement transfer

Following relay zone initiation, fault displacement increases and is transferred between the R shears by deformation within and adjacent to

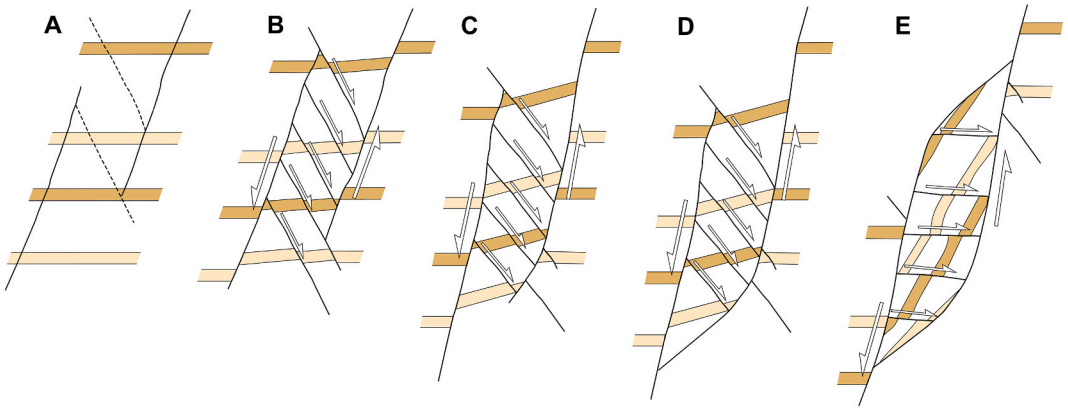

Fig. 8. Schematic representation of the possible successive stages of evolution with increasing fault displacement accumulation of a relay zone associated with Riedel-like geometries as described in this article. **A**: relay zone initiation; **B**: fault displacement transfer between adjacent fault segments; **C** to **D**: relay zone breaching and incipient synthetic rotation of bedding and antithetic faults within the relay area; **E**: relay zone double-breaching (lens development) and very evolved synthetic rotation of bedding and antithetic faults within the relay area which appear to be, respectively, sub-parallel to the lens-bounding faults and sub-horizontal to overturned.

the relay zone (Fig. 8B). The strains associated with the transfer of displacement between faults that bound a relay zone are accommodated by an increase in their throw gradient. In general the throw gradient on the relay-bounding faults is constant or varies smoothly for relay zones in either map view (i.e., relay ramps) or cross-section (e.g., Peacock and Sanderson, 1994; Childs et al., 2017; Delogkos et al., 2020). However, in contractional relay zones with a Riedel geometry the throw gradient on the R shears is stepped, with abrupt changes at branchpoints with the R′ shears (Figs. 4C and 5C). The change in throw on the R shears is equal to the throw on the abutting R′ shear (Fig. 7) which conveys that same throw increment across the relay zone to the other R shear. Each R′ shear within the relay zone therefore acts to convey an increment of throw from one bounding R shear to the other. The branchpoints at either end of an R′ shear are at different stratigraphic levels, as the branchpoint with the footwall R shear is stratigraphically lower than the branchpoint with the hangingwall R shear. Therefore the transfer of fault displacement across the relay zone via an R' shear also involves transfer between stratigraphic levels at different heights. For this reason the aggregate throw profile within the zone of overlap has an irregular shape and does not match the total throw measured on the bounding faults outside of the relay zone (Figs. 4C and 5C) in contrast to other forms of relay zone where the aggregate throw is constant in the zone of overlap.

The precise mechanism by which R′ shears convey fault displacement between R shears is not fully understood and is the subject of ongoing work. In many cases the R′ shears, and bedding within the blocks between adjacent R shears, are rotated towards the hangingwall (Figs. 3B, 4 and 5) and this block rotation is one viable mechanism for displacement transfer. To provide an indication of the effectiveness of this mechanism for displacment transfer we use a simple geometrical description that assumes the fault-bound blocks are rigid, to relate the throw magnitude on an R′ shear to the step in throw on an R shear where it is intersected by the R′ shear (Fig. 9) for a given bed/fault block rotation angle, block thickness and initial fault dip angles; the equations for calculating these R′ and 'transferred' throws are given in Fig. 9. The results of applying these equations using values of fault spacing and dip appropriate to the Ptolemais and Buzi Range structures in Figs. 4 and 5 are shown by the dashed curves in Fig. 7. In both these cases the calculated throw on the R'shears is significantly lower than the transferred throw and the calculated ratio between them is much lower than the observed 1:1 relationship. Therefore, although fault block rotation makes a contribution to displacement transfer, and this contribution becomes more significant as the initial fault dip decreases, it cannot account for the observed throw variations. Furthermore, there are several examples presented where there is no observable bed/fault

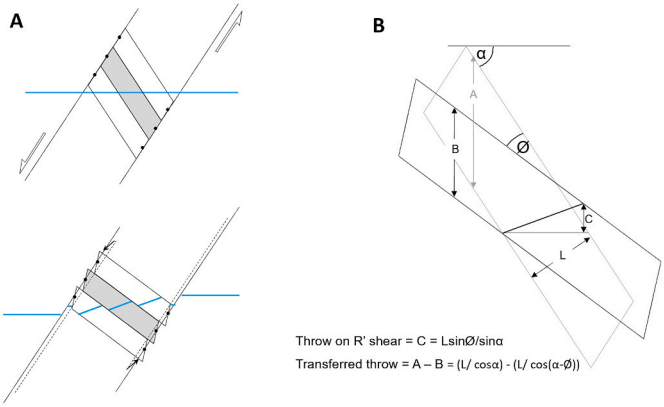

Fig. 9. Illustration of the assumptions made in calculating the relationship between the throw on R′ shears and the throw transferred between R shears by block rotation in a bookshelf style of faulting. A series of blocks separated by R′ shears with dip α and a distance L apart are rotated through Ø degrees to accommodate a tranfer of throw across the zone. During the rotation the zone widens (compare the dashed and solid line R shears in **A**) and the relay-bounding faults (i.e. the R shears) are translated as indicated by the solid arrows. We are interested in the ratio between the throw transferred across the relay zone and the throw on the R′ shears. Because this ratio is the same for the whole zone or for a single block we consider just one rotating block (**B**). The transferred throw is the change in throw on one of the bounding R shears, and is equal to the change in the apparent thickness of the zone measured in the vertical as a result of the rotation. The illustration in **B** shows that this is the difference between distances *A* and *B*. The throw on the R′ shear for an individual block is measured as the vertical component of the rotation of the initially horizontal layering, which is the distance C (in **B**). Results of these simple geometrical calculations are plotted in Fig. 7 and demonstrate that, for dips typical of normal faults, the model implies that the transferred throw is much larger than the throw on the R′ shears. This is incompatible with the observations of the natural faults, for which the two quantities are similar.

rotation but there is significant throw on the antithetic faults. There must therefore be a mode of displacement transfer via the R′ shears which is irrotational whereby the wedge of rock between a R shear and an abutting R′ shear is forced between the two shears analogous to a keystone faulting mechanism (e.g., Crosby and Crosby, 1925; Wise, 1963). This mechanism is clearly subject to significant volumetric problems at the branchpoint between the shears and these are apparent on close inspection of many of the branchpoints in the examples shown (e.g., Fig. 4A and B). It is likely that both rotational and irrotational

mechanisms are active within contractional relay zones with Riedel geometries and that their relative importance will vary with the rock properties of the host rock, strain magnitude and location. For example, bed and fault rotations are much better developed in the centre of the relay structures shown in Figs. 4 and 5 than at the top and bottom.

Pennacchioni and Mancktelow (2013) recognised the same geometrical problem related to displacment transfer across contractional relay zones. They studied contractional relay zones with antithetic Riedel shears formed in strike-slip faults in metagranitoid in the lower brittle crust (Fig. 2C). They recognised that 'the accumulated slip on the antithetic faults in the contractional stepovers is insufficient to fully account for the gradients in slip toward the tips of segmented faults' and also that the zones did not widen in the zone of overlap but neither did they show evidence for volume loss. They concluded that this 'conundrum presumably can only be resolved by significant movements out--of-plane'. While we prefer an in-plane solution, this conundrum remains a topic for further investigation.

5.3. Relay zone breaching and subsequent deformation

As the throw on a relay zone increases (Fig. 8C and D) the mechanisms for transferring fault displacement between the bounding faults may cease to operate and the relay zone becomes breached, or by-passed, by the formation of a throughgoing fault (e.g., Peacock and Sanderson, 1991, 1994; Childs et al., 1995, 2009; Cartwright et al., 1996; Crider and Pollard, 1998; Peacock, 2002; Soliva and Benedicto, 2004; Camanni et al., 2019). Relay ramps between normal faults typically breach when the fault throw is similar to, or less than, the relay zone separation (Imber et al. 2004; Soliva and Benedicto 2004; Childs et al. 2009) and contractional relay zones appear to breach at similar strains (e.g., Delogkos et al., 2020). Fig. 10A shows a fault zone with an internal structure that is typical of that seen in contractional relay zones with a Riedel geometry. However, in this case the throw across this zone is 35 m and significantly larger than the width of the fault zone (ca. 4 m). By analogy with relay zones in map view we can expect that this relay zone has breached and that the two bounding faults are connected above or below the outcrop, or both. Breaching of the relay zone is consistent with the relatively low strain within it as evidenced by the well preserved internal structure of the zone and the large angles between bedding and the R′ shears. Lack of activity on the R' shears would have occurred when one of the two bounding faults became inactive implying that the other bounding fault by-passed the relay zone to form a throughgoing fault (Fig. 8 C to **D**) when the throw was much lower than the present day throw.

The structure in Fig. 10B is similar in dimensions to that in Fig. 10A with a throw across the zone of 40 m and a fault zone width that varies between 1 and 4 m over the height of the mine face. Here again a series of antithetic faults with intervening rotated blocks is recognised but the total deformation within the zone is significantly greater, so that bedding is near parallel to the bounding faults and the antithetic faults are rotated through the horizontal to dip in the same direction as the fault-zone bounding faults. This outcrop is interpreted to be a contractional relay zone with an initial Riedel geometry which has been subjected to intense distributed shear following relay zone breaching. The R

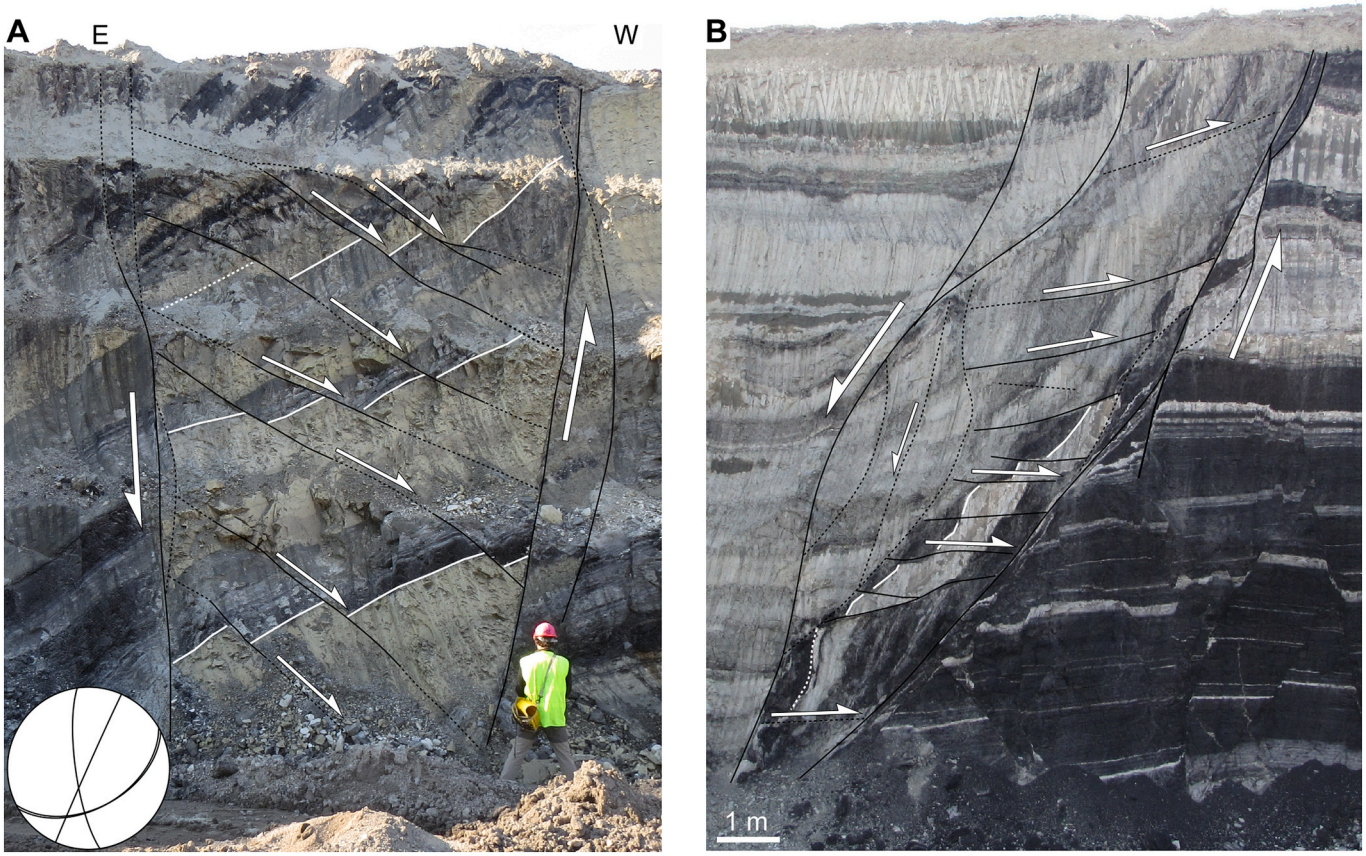

Fig. 10. Field examples of fault zones interpreted as structurally evolved relay zones with a Riedel geometry from mines in the Ptolemais Basin. The total throw across the fault zone in **A** is ca. 45 m, and includes approximately 10 m of normal drag outside the zone and 35 m of discrete throw on the two fault segments bounding the zone. Fault plane orientation data are indicated. The total throw across the fault zone in **B** is ca. 40 m. In both examples, R′ shears along with tilted layers have undergone an overall synthetic rotation. The fault zone in **A** is representative of breached Riedel relay zones in which both the bedding and the antithetic faults are shallowly dipping. The fault zone in **B** is representative of a more evolved stage (possibly a fault-bound lens) in which R′ shears are overturned and the bedding is sub-parallel to the faults bounding the zone.

shears in this case converge downwards and are projected to meet at a branchpoint ca. 2 m below the base of the outcrop. Although it cannot be demonstrated in this face, it is likely that the R shears also merge upwards, so the breached relay zone is preserved as a fault bound lens as illustrated in Fig. 8E. A similar example of rotated bedding and R' shears within a fault bound lens is provided by Nabavi et al. (2020).

We conclude that contractional relay zones with Riedel geometry follow a well defined evolutionary model similar to other relay zones along normal faults. One important difference, however, is that whilst map-view (i.e. neutral) relay zones transfer fault displacement predominantly by bed rotation, geometric considerations demonstrate that rigid block rotation alone cannot accomplish the observed displacement transfer within contractional relay zones and that other, irrotational mechanisms, are also required. The development described is specifically for contractional relay zones containing antithetic faults. It is important to note that not all contractional relay zones on normal faults contain R'shears which are more common in some settings than in others. For example, in the massive sandstone units in Moab these zones are widespread but in the Ptolemais mines R′ shears are rarely developed and ca 90% of contractional relay zones are accommodated by thinning of the marl or lignite units without the formation of additional discrete structures: examples are shown by Camanni et al. (2019) and Delogkos et al. (2020).

6. Discussion

In the previous section we presented a model for the evolution of contractional relay zones with a Riedel geometry on normal faults. The geometrical evolution of these structures is very similar to the model for evolution of Riedel shear zones that is based on classic Riedel shear models (Riedel, 1929; Tchalenko, 1970; Wilcox et al., 1973; Dooley and Schreurs, 2012) and zones of deformation bands in high porosity sandstone (e.g., Davis et al., 2000), whereby R shears broadly predate R′ shears and eventually link through the formation of P shears to form a throughgoing fault. Earlier studies have illustrated that the details of this model vary according to a number of parameters including lithology and stress conditions, and that for example, R′ shears are frequently absent (Naylor et al., 1986) or in some circumstances may predate R shears (Ahlgren, 2001). The novel aspect of this work is the description of the fault displacement distributions on R and R′ shears in a normal fault setting and the demonstration of the role of R' shears in transferring displacement between R shears. We suggest that similar displacment distributions and displacment transfer mechanisms are to be expected in zones that display the Riedel geometry, irrespective of the boundary conditions under which the geometry is produced.

Details of the development of the Riedel-like geometries vary between different areas, an outcome that appears to relate to the rheological properties of the faulted sequence. In the massive sandstones of Moab, where such geometries are very common, there is little or no evidence for the rotation of R′ shears even when fault throw is very high (Fig. 3D). This is likely to reflect the difficulty of absorbing the volumetric strains required to transfer fault displacement across contractional relay zones in these quartz-rich rocks, so that associated contractional relay zones are by-passed at low strain. By contrast, the space issues that arise at the branchpoints between R and R'shears appear to be readily resolved in other rock types, such as the marl/lignite sequence in the Ptolemais Basin and the shale-dominated Buzi Range region. In these areas both rotational and irrotational mechanisms for displacement transfer can accommodate large deformation that efficiently transfer displacement between R shears before they are by-passed.

In the classic Riedel shear zone description, R shears become connected with increasing offset to form throughgoing P shears and at higher strains the shear zone becomes a series of anastomosing shears with associated distributed deformation (e.g., Tchalenko, 1970; Dooley and Schreurs, 2012 and references therein). In the case of high strain normal fault Riedel-like geometries, increased fault displacement causes relay zone breaching but may also give rise to high internal strains to form panels of near fault-parallel bedding with strongly rotated antithetic faults (Figs. 8E and 9). The occurrence of local panels of rotated bedding within normal fault zones has been described by several authors (e.g., Rykkelid and Fossen, 2002; Ferrill et al., 2005, 2009; Ferrill and Morris, 2008; Putz-Perrier and Sanderson, 2008; Kettermann et al., 2019) and some have identified initial fault segmentation as the origin of these panels. For example, pronounced bed rotation between extensional dip relay zones has been described (Rykkelid and Fossen, 2002; Putz-Perrier and Sanderson, 2008) and identified as a mechanism for generating clay smears (Lehner and Pilaar, 1997; Vrolijk et al., 2005). Similarly, Childs et al. (2017) suggest that relay ramps between fault segments that underlap in map view can, in certain lithologies, give rise to significant synthetic bed rotation (i.e., normal drag). Here we have expanded this segmentation model to include contractional relay zones so that rotated bedding panels can occur within any of the three end-member (contractional, extensional and neutral) relay zone geometries or some intermediate between them. While it may be difficult to determine the precise origin of a particular panel of rotated bedding, we suggest that the occurrence of rotated antithetic faults, such as those in Fig. 9, may be diagnostic of a Riedel-like contractional relay zone within a normal fault.

7. Conclusions

Contractional relay zones between normal faults may be associated with multiple internal antithetic faults (i.e., R′ shears) in a Riedel-like geometry. The R shears bounding the relay zones are associated with stepped throw profiles, where portions with nearly constant throw are separated by steps in throw across branchpoints with the R′ shears. R′ shears within a relay zone have flat throw profiles that terminate abruptly at their branchpoints with the relay-bounding R shears. The constant throw on individual R′ shears roughly coincides with the steps in throw where they intesect a relay-bounding R shear, so that R′ shears convey throw across the relay zone. Fault displacement is transferred across these contractional relay zones by a combination of rotational and irrotational mechanisms. When relay zones become breached and the mechanism of throw transfer becomes inactive, the Riedel fault geometry may be preserved intact within the fault zone or may be deformed by progressive shearing and rotation of bedding and the R′ shears within a fault-bound panel. The occurrence of antithetic Riedel shears between normal faults may be indicative of the presence of an intact or failed contractional relay zone. The geometries of Riedel shears encountered at contractional relay zones in normal faults can also be found associated with other faulting modes and displacement transfer via R' shears idenitified here may occur in all faulting modes.

Author statement

Giovanni Camanni: Conceptualization; Data curation; Formal analysis; Investigation; Visualization; Methodology; Writing - original draft. **Conrad Childs**: Conceptualization; Investigation; Methodology; Supervision; Funding acquisition; Project administration; Writing - review & editing. **Efstratios Delogkos**: Conceptualization; Investigation; Methodology; Writing - review & editing. **Vincent Roche**: Investigation; Methodology; Writing - review & editing. **Tom Manzocchi**: Investigation; Supervision; Funding acquisition; Project administration; Writing - review & editing. **John Walsh**: Investigation; Supervision; Funding acquisition; Project administration; Writing - review & editing.

Declaration of competing interest

The authors declare that they have no known competing financial interests or personal relationships that could have appeared to influence the work reported in this paper.

Data availability

Data will be made available on request.

Acknowledgments

This work was carried out in the frame of the consortium-sponsored project QUAFF brokered by the Industry Technology Facilitator, and funded by Anadarko, ConocoPhillips (UK), Eni, ExxonMobil, Marathon Oil Corporation, Shell (UK), Equinor, Total E&P UK and Woodside Energy; representatives of the sponsor companies are thanked for their insightful comments throughout the research. This publication has also partly emanated from work supported by a research grant from Science Foundation Ireland (SFI) under Grant Number 13/RC/2092 and co-funded under the European Regional Development Fund. E. Delogkos is funded by the Irish Research Council under grant number GOIPD/2020/530, and V. Roche by the European Union's Horizon 2020 research and innovation programme under the Marie Sklodowska-Curie grant agreement No 884931. Fig. 5 was created using ArcGIS® software by Esri and the World Imagery data (sources: Esri, DigitalGlobe, GeoEye, i-cubed, USDA FSA, USGS, AEX, Getmapping, Aerogrid, IGN, IGP, swisstopo, and the GIS User Community) provided within the software. ArcGIS® and ArcMap™ are the intellectual property of Esri and are used herein under license 594166 kindly provided to the University of Napoli Federico II. Copyright © Esri. All rights reserved. Four anonymous reviewers and the editor Fabrizio Agosta are thanked for their constructive comments on this work.

Appendix A. Supplementary data

Supplementary data to this article can be found online at https://doi.org/10.1016/j.jsg.2023.104827.

References

Ahlgren, S.G., 2001. The nucleation and evolution of Riedel shear zones as deformation bands in porous sandstone. J. Struct. Geol. 23.
Antonellini, M., Aydin, A., 1995. Effect of faulting on fluid fow in porous sandstones: geometry and spatial distribution. AAPG (Am. Assoc. Pet. Geol.) Bull. 79, 642–671.
Arboleya, M.L., Engelder, T., 1995. Concentrated slip zones with subsidiary shears: their development on three scales in the Cerro Brass fault zone, Appalachian valley and ridge. J. Struct. Geol. 17, n4.
Back, S., Morley, C.K., 2016. Growth faults above shale - seismic-scale outcrop analogues from the Makran foreland, SW Pakistan. Mar. Petrol. Geol. 70, 144–172.
Camanni, G., Roche, V., Childs, C., Manzocchi, T., Walsh, J., Conneally, J., Saqab, M.M., Delogkos, E., 2019. The three-dimensional geometry of relay zones within segmented normal faults. J. Struct. Geol. 129, 103895.
Camanni, G., Vinci, F., Tavani, S., Ferrandino, V., Mazzoli, S., Corradetti, A., Parente, M., Iannace, A., 2021. Fracture density variations within a reservoir-scale normal fault zone: a case study from shallow-water carbonates of southern Italy. J. Struct. Geol. 151.
Carpentier, S.F.A., Green, A.G., Langridge, R., Boschetti, S., Doetsch, J., Abächerli, A.N., Horstmeyer, H., Finnemore, M., 2012. Flower structures and Riedel shears at a step over zone along the Alpine Fault (New Zealand) inferred from 2-D and 3-D GPR images. J. Geophys. Res. 117, B02406 https://doi.org/10.1029/2011JB008749.
Cartwright, J.A., Mansfield, C., Trudgil, B., 1996. The growth of normal faults by segment linkage. Geological Society, London, Special Publications 99, 163–177.
Cembrano, J., González, G., Arancibia, G., Ahumada, I., Olivares, V., Herrera, V., 2005. Fault zone development and strain partitioning in an extensional strike-slip duplex: a case study from the Mesozoic Atacama fault system, Northern Chile. Tectonophysics 400, 1–4.
Childs, C., Watterson, J., Walsh, J.J., 1995. Fault overlap zones within developing normal fault systems. J. Geol. Soc. 152, 535–549.
Childs, C., Manzocchi, T., Walsh, J.J., Bonson, C.G., Nicol, A., Schöpfer, M.P.J., 2009. A geometric model of fault zone and fault rock thickness variations. J. Struct. Geol. 31, 117–127.
Childs, C., Manzocchi, T., Nicol, A., Walsh, J.J., Soden, A.M., Conneally, J., Delogkos, E., 2017. The relationship between normal drag, relay ramp aspect ratio and fault zone structure. In: Childs, C., Holdsworth, R.E., Jackson, C.A.-L., Manzocchi, T., Walsh, J. J., Yielding, G. (Eds.), The Geometry and Growth of Normal Faults, 439. Geological Society of London, Special Publication. https://doi.org/10.1144/SP439.16.
Cloos, H., 1928. Experimente zur inneren Tektonik. Centralblatt für Mineralogie 12, 609–621.
Crider, J.G., Pollard, D.D., 1998. Fault linkage: three-dimensional mechanical interaction between echelon normal faults. J. Geophys. Res. Solid Earth 103, 24373–24391.
Crosby, W.O., Crosby, I.B., 1925. Keystone faults. Bull. Geol. Soc. Am. 36 (4), 623–640.
Davis, G.H., 1999. Structural Geology of the Southern Utah Parks and Monuments Region, Colorado Plateau, with Special Emphasis on Deformation Band Shear Zones, 342. Geological Society of America Special Paper, p. 158.
Davis, G.H., Bump, A.P., Garcia, P.E., Ahlgren, G.G., 2000. Conjugate Riedel deformation band shear zones. J. Struct. Geol. 22, 169–190.
Delogkos, E., Childs, C., Manzocchi, T., Walsh, J.J., Pavlides, S., 2017a. The role of bed-parallel slip in the development of complex normal fault zones. J. Struct. Geol. https://doi.org/10.1016/j.jsg.2017.02.014.
Delogkos, E., Manzocchi, T., Childs, C., Sachanidis, C., Barbas, T., Schöpfer, M.P., Chatzipetros, A., Pavlides, S., Walsh, J.J., 2017b. Throw partitioning across normal fault zones in the Ptolemais Basin, Greece. In: Childs, C., Holdsworth, R.E., Jackson, C.A.-L., Manzocchi, T., Walsh, J.J., Yielding, G. (Eds.), The Geometry and Growth of Normal Faults, 439. Geological Society of London, Special Publication.
Delogkos, E., Childs, C., Manzocchi, T., Walsh, J.J., 2018. The nature and origin of bed-parallel slip in Kardia mine, Ptolemais Basin, Greece. J. Struct. Geol. 113, 115–133.
Delogkos, E., Manzocchi, T., Childs, C., Camanni, G., Roche, V., 2020. The 3D structure of a normal fault from multiple outcrop observations. J. Struct. Geol. 136.
Diamanti, R., Camanni, G., Natale, J., Vitale, S., 2022. A gravitational origin for volcano-tectonic faults in the Campi Flegrei caldera (southern Italy) inferred from detailed field observations. J. Struct. Geol. 161.
Dooley, T.P., Schreurs, G., 2012. Analogue modelling of intraplate strike-slip tectonics: a review and new experimental results. Tectonophysics 574 (575), 1–71.
Ellouz-Zimmermann, N., Deville, E., Müller, C., Lallemant, S., Subhani, A.B., Tabreez, A. R., 2007. Impact of sedimentation on convergent margin tectonics: example of the makran accretionary prism (Pakistan). In: Lacombe, O., Roure, F., Lavé, J., Vergés, J. (Eds.), Thrust Belts and Foreland Basins. Frontiers in Earth Sciences. Springer, Berlin, Heidelberg.
Faulkner, D.R., Lewis, A.C., Rutter, E.H., 2003. On the internal structure and mechanics of large strike-slip fault zones: field observations of the Carboneras fault in southeastern Spain. Tectonophysics 367. Issues 3–4.
Faulkner, D.R., Mitchell, T.M., Rutter, E.H., Cembrano, J., 2008. On the structure and mechanical properties of large strike-slip faults. Geological Society, London, Special Publications 299, 139–150.
Ferrill, D.A., Morris, A.P., 2008. Fault zone deformation controlled by carbonate mechanical stratigraphy, Balcones fault system, Texas. AAPG (Am. Assoc. Pet. Geol.) Bull. 92, 3.
Ferrill, D.A., Morris, A.P., Sims, D.W., Waiting, D.J., Hasegawa, S., 2005. Development of synthetic layer dip adjacent to normal faults. In: Sorkhabi, R., Tsuji, Y. (Eds.), Faults, Fluid Flow, and Petroleum Traps: American Association of Petroleum Geologists Memoir 85, pp. 125–138.
Ferrill, D.A., Morris, A.P., McGinnis, R.N., 2009. Crossing conjugate normal faults in field exposures and seismic data. AAPG (Am. Assoc. Pet. Geol.) Bull. 93, 11.
Ferrill, D.A., Morris, A.P., McGinnis, R.N., Smart, K.J., Ward, W.C., 2011. Fault zone deformation and displacement partitioning in mechanically layered carbonates: the Hidden Valley fault, central Texas. AAPG (Am. Assoc. Pet. Geol.) Bull. 95, 1383–1397.
Foxford, K.A., Garden, I.R., Guscott, S.C., Burley, S.D., Lewis, J.J.M., Walsh, J.J., Watterson, J., 1996. In: Huffman, A.C., Lund, W.R., Godwin (Eds.), Geology and Resources of the Paradox Basin, the Field Geology of the Moab Fault, Utah Geological Society Guidebook, 25. L. H., pp. 265–283
Foxford, K.A., Walsh, J.J., Watterson, J., Garden, I.R., Guscott, S.C., Burley, S.D., 1998. Structure and content of the Moab Fault Zone, Utah, USA, and its implications for fault seal prediction. Geological Society, London, Special Publications 147, 87–103.
Gent, H.v., Urai, J.L., 2019. Abutting faults: a case study of the evolution of strain at Courthouse branch point, Moab Fault, Utah. Solid Earth 11, 513–526.
Imber, J., Tuckwell, G.W., Childs, C., Walsh, J.J., Manzocchi, T., Heath, A.E., Bonson, C. G., Strand, J., 2004. Three-dimensional distinct element modelling of relay growth and breaching along normal faults. J. Struct. Geol. 26 (10), 1897–1911.
Katz, J., Weinberger, R., Aydin, A., 2004. Geometry and kinematic evolution of Riedel shear structures, capitol reef national park, Utah. J. Struct. Geol. 26, 491–501.
Kettermann, M., Weismüller, C., von Hagke, C., Reicherter, K., Urai, J.L., 2019. Large near-surface block rotations at normal faults of the Iceland rift: evolution of tectonic caves and dilatancy. Geology 47, 781–785.
Kim, Y.S., Peacock, D.C.P., Sanderson, D.J., 2003. Mesoscale strike-slip faults and damage zones at Marsalforn, Gozo Island, Malta. J. Struct. Geol. 25 (5), 793–812.
Lehner, F.K., Pilaar, W.F., 1997. The Emplacement of Clay Smears in Synsedimentary Normal Faults: Inferences from Field Observations Near Frechen, Germany, 7. In Norwegian Petroleum Society Special Publications, pp. 39–50 (Elsevier).
Mandl, G., 1987. Tectonic deformation by rotating parallel faults: the "bookshelf' mechanism. Tectonophysics 141, 4.
Martel, S.J., Pollard, D.D., Segall, P., 1988. Development of Simple Strike-Slip Fault Zones, Mount Abbot Quadrangle, Sierra Nevada, California, 100. Geological Society of America Bullettin, pp. 1451–1465.
Nabavi, S.T., Alavi, S.A., Wibberley, C.A.J., Jahangiri, M., 2020. Normal fault networks and their spatial relationships in Plio-Quaternary sedimentary series: a case study in the Zanjan Depression, NW Iran. J. Struct. Geol. 136.
Naylor, M.A., Mandl, G., Sijpesteijn, C.H.K., 1986. Fault geometries in basement-induced wrench faulting under different initial stress states. J. Struct. Geol. 8, 737–752.
Nicholson, C., Seeber, L., Williams, P., Sykes, L.R., 1986. Seismic evidence for conjugate slip and block rotation within the San Andreas fault system, Southern California. Tectonics 5 (4), 629–648.
Nicol, A., Childs, C., Walsh, J.J., Schafer, K.W., 2013. A geometric model for the formation of deformation band clusters. J. Struct. Geol. 55, 21–33.
Nixon, C.V., Vaagan, S., Sanderson, D.J., Gawthorpe, R.L., 2018. Spatial distribution of damage and strain within a normal fault relay at Kilve. U.K. J. Struct. 118, 194–209.

Okubo, C.H., Schultz, R.A., 2005. Evolution of damage zone geometry and intensity in porous sandstone: insight gained from strain energy density. J. Geolog. Soc. London. 162.
Pavlides, S.B., Mountrakis, D.M., 1987. Extensional tectonics of northwestern Macedonia, Greece, since the late Miocene. J. Struct. Geol. 9, 385–392.
Peacock, D.C.P., 2002. Propagation, interaction and linkage in normal fault systems. Earth Sci. Rev. 58, 121–142.
Peacock, D.C.P., Sanderson, D.J., 1991. Displacements, segment linkage and relay ramps in normal fault zones. J. Struct. Geol. 13 (6), 721–733.
Peacock, D.C.P., Sanderson, D.J., 1994. Geometry and development of relay ramps in normal fault systems. AAPG (Am. Assoc. Pet. Geol.) Bull. 78, 147–165.
Pennacchioni, G., Mancktelow, N.S., 2013. Initiation and Growth of Strike-Slip Faults within Intact Metagranitoid (Neves Area, Eastern Alps, Italy), 125. GSA Bulletin.
Platt, J., Legett, J.K., Alam, S., 1988. Slip vectors and fault mechanics in the Makran accretionary wedge, SW Pakistan. Geology 13.
Pucci, S., Pantosti, D., Barchi, M.R., Palyvos, N., 2007. A complex seismogenic shear zone: the Düzce segment of North Anatolian Fault (Turkey). Earth Planet Sci. Lett. 262. Issues 1–2.
Putz-Perrier, M.W., Sanderson, D.J., 2008. Spatial distribution of brittle strain in layered sequences. J. Struct. Geol. 30, 50–64.
Quigley, M., Van Dissen, R., Villamor, P., Litchfield, N., Barrell, D., Furlong, K., Stahl, T., Duffy, B., Bilderback, E., Noble, D., Townsend, D., Begg, J., Jongens, R., Ries, W., Claridge, J., Klahn, A., Mackenzie, H., Smith, A., Hornblow, S., Nicol, R., Cox, S., Langridge, R., Pedley, K., 2010. Surface rupture of the greendale fault during the Darfield (canterbury) earthquake, New Zealand. Bull. N. Z. Soc. Earthq. Eng. 43 (4), 236–242.
Quigley, M., Van Dissen, R., Litchfield, N., Villamor, P., Duffy, B., Barrell, D., Furlong, K., Stahl, T., Bilderback, E., Noble, D., 2012. Surface rupture during the 2010 Mw7.1 Darfield (Canterbury) earthquake: implications for fault rupture dynamics and seismic-hazard analysis. Geology 40 (1), 55–58.
Ren, J., Zhang, Z., Gai, H., Kang, W., 2021. Typical Riedel shear structures of the coseismic surface rupture zone produced by the 2021 Mw 7.3 Maduo earthquake, Qinghai, China, and the implications for seismic hazards in the block interior. Nat. Haz. Res. 1 (4).
Richard, P.D., Naylor, M.A., Koopman, A., 1995. Experimental models of strike-slip tectonics. Petrol. Geosci. 1, 71–80.
Riedel, W., 1929. Zur Mechanik Geologischer Brucherscheinungen Centralblatt Mineralogie, pp. 354–368. Abteilung.
Roche, V., Childs, C., Madritsch, H., Camanni, G., 2020. Layering and structural inheritance controls on fault zone structure in three dimensions: a case study from the northern Molasse Basin, Switzerland. J. Geol.Soc. 177, 493–508.
Roche, V., Camanni, G., Childs, C., Manzocchi, T., Walsh, J., Conneally, J., Saqab, M.M., Delogkos, E., 2021. Variability in the three-dimensional geometry of segmented normal fault surfaces. Earth Sci. Rev. 216.
Rykkelid, E., Fossen, H., 2002. Layer rotation around vertical fault overlap zones: observations from seismic data, field examples, and physical experiments. Mar. Petrol. Geol. 19, 181–192.
Schultz, R.A., Balasko, C.M., 2003. Growth of deformation bands into echelon and ladder geometries. Geophys. Res. Lett. 30, 20.
Segall, P., Pollard, D.D., 1980. Mechanics of discontinuous faults. J. Geophys. Res. 85, 4337–4350.
Soliva, R., Benedicto, A., 2004. A linkage criterion for segmented normal faults. J. Struct. Geol. 26 (12), 2251–2267.
Stanton-Yonge, A., Cembrano, J., Griffith, W.A., Jensen, E., Mitchell, T.M., 2020. Self-similar length-displacement scaling achieved by scale-dependent growth processes: evidence from the Atacama Fault System. J. Struct. Geol. 133.
Tapponnier, P., Armijo, R., Manighetti, I., Courtillot, V., 1990. Bookshelf faulting and horizontal block rotations between overlapping rifts in Southern Afar. Geophys. Res. Lett. 17 (1), 1–4.
Tchalenko, J.S., 1970. Similarities between shear zones of different magnitudes. Geol. Soc. Am. Bull. 81, 1625–1640.
Tchalenko, J.S., Ambraseys, N.N., 1970. Structural analysis of the dasht-e bayaz (Iran) earthquake fractures. GSA Bulletin 81 (1), 41–60.
Terres, R.R., Sylvester, A.G., 1981. Kinematic analysis of rotated fractures and blocks in simple shear. Bull. Seismol. Soc. Am. 71 (5), 1593–1605.
Tondi, E., Antonellini, M., Aydin, A., Marchegiani, L., Cello, G., 2006. The role of deformation bands, stylolites and sheared stylolites in fault development in carbonate grainstones of Majella Mountain, Italy. J. Struct. Geol. 28 (3), 376–391.
Vrolijk, P., Myers, R., Sweet, M.L., Shipton, Z.K., Dockrill, B., Evans, J.P., Heath, J., Williams, A.P., 2005. Anatomy of reservoir-scale normal faults in central Utah: stratigraphic controls and implications for fault zone evolution and fluid flow. Interior Western United States 6, 261.
Wilcox, R.E., Harding, T.P., Seely, D.R., 1973. Basic Wrench Tectonics, 57. The American Association of Petroleum Geologists Bullettin, p. 1.
Wise, D.U., 1963. Keystone faulting and gravity sliding driven by basement uplift of Owl Creek Mountains, Wyoming. AAPG (Am. Assoc. Pet. Geol.) Bull. 47 (4), 586–598.
Zaky, K.S., 2017. fault zone architecture within miocene–pliocene syn-rift sediments, northwestern red sea, Egypt. J. Earth Syst. Sci. 126.